A Process to Simulate GNSS-R Delay-Doppler Map of Tsunami-dominant Sea Surface

Qingyun Yan, *Student Member, IEEE*, and Weimin Huang, *Senior Member, IEEE*
Faculty of Engineering and Applied Science, Memorial University
St.John's, Newfoundland, Canada
Email: {qy2543, weimin}@mun.ca

***Abstract*—In this paper, a process is presented to simulate Global Navigation Satellite System-Reflectometry (GNSS-R) delay-Doppler maps (DDMs) of a tsunami-dominant sea surface. In this method, the bistatic scattering Z-V model, the sea surface mean square slope model of Cox and Munk and the tsunami-induced wind perturbation model are employed. By taking advantage of the first two models, the DDMs of tsunami-free region can be simulated. In order to accomplish the DDM simulation of tsunami-dominant surface, the tsunami-induced wind perturbation model is utilized on top of that. The simulations of the scattering coefficient distribution and the corresponding DDMs of a fixed region of interest before and during the tsunami are exhibited. On the final stage of analysis, by subtracting the simulation results that are free of tsunami from simulations with presence of tsunami, the tsunami-induced variations can be clearly observed. The process is implemented based on the 2004 Sumatra-Andaman tsunami.**

I. INTRODUCTION

It has been widely recognized that tsunamis are one of the worst natural hazards. For example, the tsunami triggered by the 2004 Indian Ocean earthquake killed many people and caused tremendous damage to several countries [1]. Thus, tsunami detection is especially important. The conventional buoy measurement may be a costly and inefficient method of tsunami detection due to its high cost and low coverage [1]. The altimeter satellite may provide some direct information about the tsunami such as sea surface height (SSH) and radar backscattering coefficient. For instance, Jason-1 satellite altimeter encountered the 2004 Sumatra-Andaman tsunami on its path 109 for cycle 129, thereby offering valuable data on tsunami measurement [2]. However, only a handful of definitive SSH changes caused by tsunamis have been reported out of more than 150 documented tsunami events since the launch of the TOPEX/Poseidon satellite altimeter in 1992 [3]. Recently, GNSS-R has emerged as an efficient and accurate technique for sea surface remote sensing [4], which shows advantages in both temporal and spatial coverage and immunity to weather effects [4]. GNSS-R has been successfully used for ocean altimetry, sea surface wind sensing, ice and land surfaces sensing [4]. However, there are very few reports in the literature about the GNSS-R DDM based tsunami detection. In this paper, a process for simulating tsunami-dominant sea surface DDM is proposed.

II. MODEL IMPLEMENTATION AND SIMULATION PROCESS

The Cox and Munk model [5] and the Zavorotny and Voronovich (Z-V) model [6] have already been used to simulate the GNSS-R DDM of sea surface (e.g., [7], [8]). The Z-V model depicts the scattered GPS signal power as a function of the time delay and Doppler frequency shift, elevation angle of the transmitter and the height of the receiver as well as the surface scattering coefficient (σ^0). In practice, except σ^0, the rest of the factors in the Z-V model are regarded as known. The Cox and Munk model substantiates an empirical relationship between the wind speed at the height of 10 m above the sea surface (U_{10}) and the sea surface mean square slope (MSS). Consequently, the sea surface scattering coefficient σ^0 is determined by MSS [8]. In summary, with the knowledge of U_{10} over sea surface, the corresponding DDM can be simulated by combining the Cox and Munk model and the Z-V model. With this in mind, it can be expected that if the wind field over a tsunami-dominant sea surface is available, the corresponding DDM can be simulated. In fact, the wind speed during a tsunami event can be derived from the tsunami-induced wind speed perturbation model [2].

It should be noted that the tsunami-induced wind speed perturbation model [2] has been successfully applied in the simulation of radar backscattering strength (e.g., [3]) over the tsunami region. This model shows that the effective wind speed during a tsunami event is dependent on the tsunami parameters, and distinguishes from the background wind speed by a factor [2]

$$M = 1 - \frac{\kappa a c}{H u_* \ln \beta} \tag{1}$$

where $\kappa = 0.4$, $u_* = 0.04U_{10}$, H is the height of the background logarithmic boundary layer, a is the sea surface height change due to the tsunami, $c = \sqrt{gD}$ is tsunami phase speed, where g is the acceleration due to gravity, D is the depth of sea. Moreover,

$$\beta = \frac{\kappa u_* T_0}{2\pi z_0} \tag{2}$$

$z_0 = 0.01u_*^2/g$ is the roughness length, and T_0 is the tsunami period.

By employing these models, the wind speed distribution during a tsunami can be simulated with different tsunami parameters and background wind speed. Then, the same process presented in [7], which simulates the DDM for a tsunami-free sea, can be used to generate the DDM for a tsunami event.

III. SIMULATION RESULTS

The parameters associated with tsunami DDM simulation are chosen based on the 2004 Sumatra-Andaman tsunami.

978-0-933957-43-5 ©2015 MTS

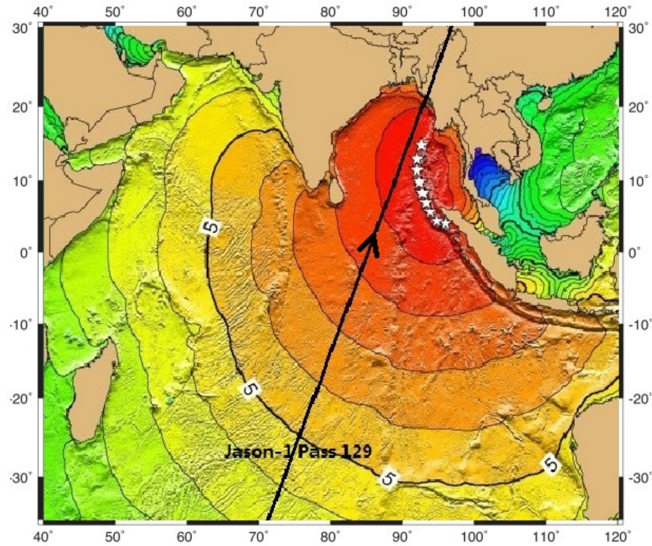

Fig. 1. Jason-1 satellite altimeter ground track during the 2004 Sumatra-Andaman tsunami. Black line indicates the Jason-1 ground track with a direction in accordance with the arrow. White stars represent the epicentre. Contours of the tsunami leading front are also shown with hourly intervals. (This graphic is the work of the National Geophysical Data Center/NOAA, adopted from http://www.ngdc.noaa.gov/hazard/img/2004_1226.jpg).

A. Simulation Scenario Setup

The Jason-1 satellite altimeter encountered the tsunami (115 min after the earthquake appeared) on the morning of 26 December 2004 [2] (shown in Fig. 1). It provided valuable data on tsunami measurement [2]. The SSH measured by Jason-1 on cycle 109 during the tsunami event is subtracted by the average SSH observed over the exactly same ground track on cycles 108 and 110 and the difference is regarded as tsunami-induced SSH change a (shown in Fig. 2*a*). This process is in accord with [9]. Besides, it has been reported in [9] that the tsunami-induced SSH change a over the range from (5.00°S, 83.96°E) to (1.00°N, 86.12°E) can be well fitted by a sine wave with a wavelength of 580 km and an amplitude of 60 cm (see Fig. 2*a*). For a better illustration purpose, values of the fitted sine model is used as a in (1) for our simulation. In addition, a is assumed to distribute uniformly along the contours of the tsunami leading wave front which are concentric circles with a center at the epicenter (3.4° N, 94.2° E).

The U_{10} measurement from QuikSCAT on its orbit 28744 is considered to be the background wind speed. It recorded the wind speed right before the earthquake (around 45 min ahead) over the region with presence of the later tsunami (also containing of the Jason-1 ground track), which means this measurement is totally free of the tsunami perturbation. Therefore, it is reasonable to regard QuikSCAT measurement as background U_{10}. Incidentally, QuikSCAT makes two-dimensional U_{10} measurement.

Here, to facilitate the simulation, for the rest of the parameters in (1) and (2), the typical empirical values are adopted in align with [2] that $T_0 = 40$ min, $D = 4000$ m and $H = 60$ m. With the knowledge of the SSH change a due to the tsunami and the background wind speed, the effective wind speed over a tsunami surface can therefore be determined by implementing the tsunami-induced wind speed perturbation model. For comparison, the effective U_{10} is calculated based on QuikSCAT measurement over the Jason-1 ground track. The measured (solid-line) and simulated (dash-line) effective U_{10} during the tsunami are shown in Fig. 2*b*. A slight inconformity can be noticed and this may be due to the variances of background U_{10} during the course of 160 minutes (the time gap between the measurements of QuikSCAT and Jason-1).

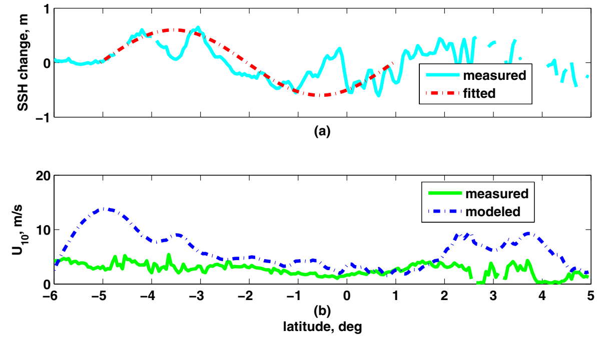

Fig. 2. Jason-1 measurement for pass 129 from (6.00°S, 83.60°E) to (4.99°N, 87.54°E) obtained during the 2004 tsunami (a) SSH change due to a tsunami. (b) Tsunami-dominant sea surface U_{10}. Gaps in the curves are caused by deficiency of measured data.

TABLE I. TSUNAMI DDM SIMULATION SETTING UP

Simulation parameters	Value (Data source)
Tsunami period (T_0)	40 min
Depth of ocean (D)	4000 m
Height of the background logarithmic boundary layer (H)	60 m
SSH change (a)	Fitted sine wave model
Background wind speed	QuikSCAT measurement on orbit 28744
Transmitter height	20000 km
Receiver height	680 km
Transmitter velocity	(-2.72, 2.68, -.65) km/s
Receiver velocity	(7.21, 1.23, 1.72) km/s
SP position	(6.0081° S, 83.6019° E)

The parameters mentioned above are tabulated in Table I. In terms of GNSS-R simulation scenario, the parameters used in [10] are adopted and also shown in Table I.

In order to manifest a unique influence from the tsunami on GNSS-R sea surface remote sensing in this work, a continuous detection over a fixed region of interest is assumed, which is set around (6.0081° S, 83.6019° E) with a size of 200 km by 200 km. To achieve this, both of the transmitter and the receiver are set fixed over time. In this fashion, the variations caused by the geometry change of GNSS-R system will be eliminated as well, which allows a more direct inspection on tsunami effect. At 02:55:22 UT, this region was free from tsunami and the observation result at this time will be regarded as initial. The initial simulation only depends on the background U_{10} over this region measured by QuikSCAT. However, within a few minutes, this region experienced a tsunami passage. With the tsunami entering into this region, tsunami-induced wind speed perturbation model must be applied. The effective U_{10} will be calculated based on this model with the knowledge of background U_{10} and a. As $D = 4000$ m is assumed, the tsunami propagation speed can thus be approximated by 200 m/s. Meanwhile, the SSH change in Fig. 2*a* is regarded as initial distribution. For this reason, the a over this region at each moment can be easily deduced according to the distance and tsunami propagation speed, so does the effective U_{10}.

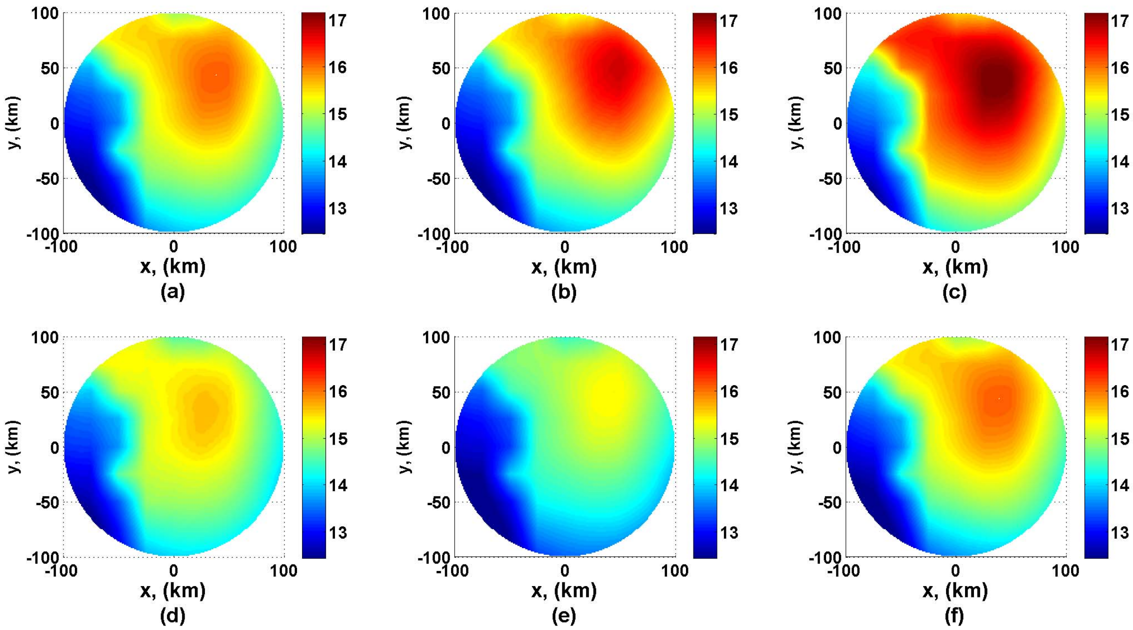

Fig. 3. Simulated σ^0 without and with tsunami detected using fitted sine wave as input a: (a) without tsunami; (b) with a part of tsunami leading front; (c) with the tsunami crest; (d) with a part between the crest and trough; (e) with the tsunami trough; (f) with the tail of tsunami tsunami leading front.

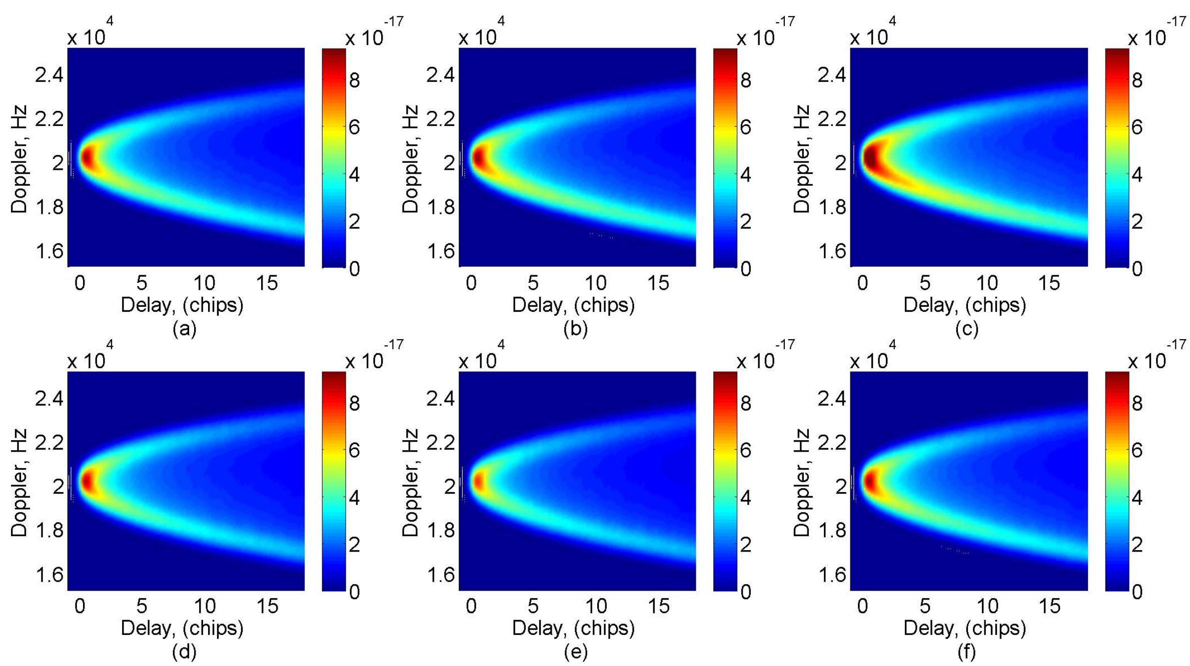

Fig. 4. Corresponding DDMs associated with σ^0 in Figure 3

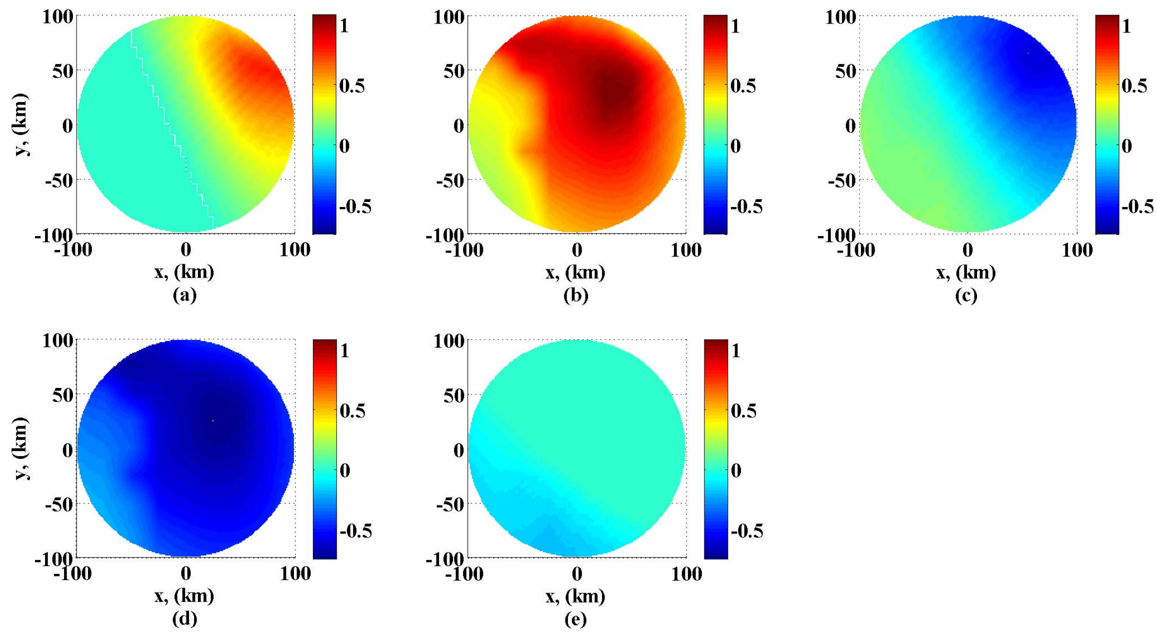

Fig. 5. Differences of σ^0 between simulations with tsunami and without: (a) with a margin of tsunami leading front; (b) with the tsunami crest; (c) with transition part between the crest and trough; (d) with the tsunami trough; (e) with the tail of tsunami leading front.

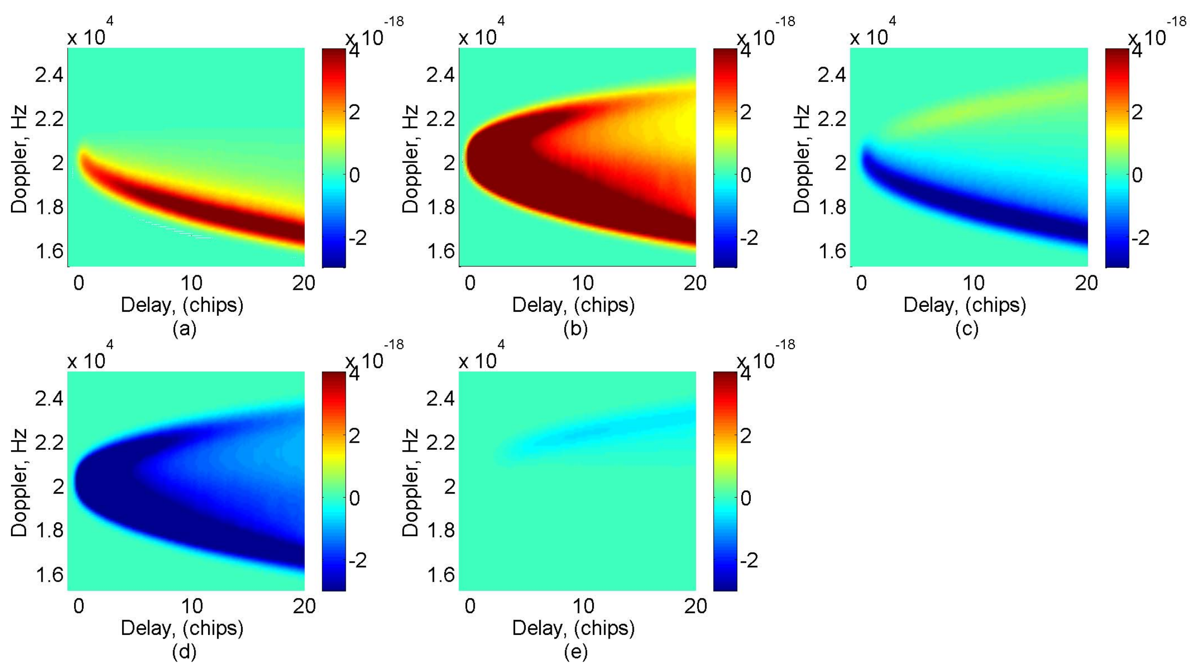

Fig. 6. Differences between tsunami DDMs and tsunami-free DDM

B. Results

The simulation results of σ^0 and corresponding DDMs are exhibited in Fig. 3 and Fig. 4, respectively. The time gaps with respect to the initial detection of each sub-plot from Fig. 3*a* to Fig. 3*f* are: 0, 9.17 min, 22.92 min, 36.67 min, 50.42 min and 64.17 min, respectively. Fig. 4 shows the corresponding DDM simulations associated with σ^0 in Fig. 3. In order to manifest the tsunami-induced variations in σ^0 and DDMs, simulations with tsunami are subtracted by the initial one that contains no tsunami, i.e., sub-plots (*b*) - (*f*) in both Fig. 3 and Fig. 4 are subtracted by the corresponding sub-plot (*a*). The resultant scattering coefficient and DDM differences are displayed in Fig. 5 and Fig. 6, respectively. In Fig. 5, the σ^0 variations caused by the tsunami are found to be ± 1 dB. This result is consistent with the estimation in [2].

Intuitively, a rising a will lead to a reductive M factor according to (1). On the other side, a decreasing U_{10} will contribute to an increase in σ^0. On the whole, the variances in σ^0 are coincident with the changes of a. Therefore, the passage of the tsunami can be indicated from Fig. 5: a) the leading front appeared first; b) then came the crest; c) the transition region between the crest and the trough approached later; d) after that, the trough could be expected; e) finally, the tsunami wave propagated out of this region with only a small portion of tail remained. The variations in σ^0 are approximately proportional to the tsunami-induced SSH changes. The tsunami-induced variances in DDMs can be observed in Fig. 6.

IV. Conclusion

In this work, a process is proposed to simulate the DDM of tsunami-dominant sea surface. The Z-V model, the Cox and Munk model and the tsunami-induced wind speed perturbation model are employed in this method. The simulations of the scattering coefficient distribution and the corresponding DDMs are presented. The σ^0 variations caused by the tsunami are found to be ± 1 dB, which is consistent with the estimation in [2]. Finally, by studying the tsunami-induced variations in σ^0, the passage of tsunami can be clearly observed. In the future, retrieving tsunami parameters from the simulated DDMs of tsunami-dominant sea surface will be investigated.

Acknowledgment

This work was supported by the Natural Sciences and Engineering Research Council of Canada Discovery Grant (NSERC 402313-2012) to Dr. W. Huang.

References

[1] K. Yu, "Tsunami-wave parameter estimation using GNSS-based sea surface height measurement," *IEEE Trans. Geosci. Remote Sens.*, vol. 53, no. 5, pp. 2603-2611, May. 2015.

[2] O. A. Godin, V. G. Irisov, R. R. Leben, B. D. Hamlington, and G. A. Wick, "Variations in sea surface roughness induced by the 2004 Sumatra-Andaman tsunami," *Nat. Hazards Earth Syst. Sci.*, no. 9, pp. 1135-1147, Jul. 2009.

[3] B. D. Hamlington, R. R. Leben, O. A. Godin, and V. G. Irisov, "On the feasibility of tsunami detection using satellite-based sea surface roughness measurements," in *Proc. IEEE Int. Geosci. Remote Sens. Symp.*, Honolulu, HI, USA, pp. 3035-3038, Jul. 2010.

[4] S. Jin, G. P. Feng, and S. Gleason, "Remote sensing using GNSS signals: Current status and future directions," *Adv. Space Res.*, vol. 47, no. 10, pp. 1645-1653, May. 2011.

[5] C. Cox and W. Munk, "Measurement of the roughness of the sea surface from photographs of the sun's glitter," *J. Opt. Soc. Amer.*, vol. 44, pp. 838-850, Nov. 1954.

[6] V. U. Zavorotny and A. G. Voronovich, "Scattering of GPS signals from the ocean with wind remote sensing application," *IEEE Trans. Geosci. Remote Sens.*, vol. 38, no. 2, pp. 951-964, Mar. 2000.

[7] M. P. Clarizia *et al.*, "Analysis of GNSS-R delay-Doppler maps from the UK-DMC satellite over the ocean," *IEEE Geosci. Remote Sens. Lett.*, vol. 36, 02608, 2009.

[8] C. Li and W. Huang, "An algorithm for sea surface wind field retrieval from GNSS-R delay-Doppler map," *IEEE Geosci. Remote Sens. Lett.*, vol. 11, no. 12, pp. 2110-2114, Dec. 2014.

[9] J. Gower, "The 26 December 2004 tsunami measured by satellite altimetry," *Int. J. Remote Sens.*, vol. 28, Nos. 13-14, pp. 2897-2913, 2007.

[10] C. Li, W. Huang and S. Gleason, "Dual antenna space-Based GNSS-R ocean surface mapping: Oil slick and tropical cyclone sensing," *IEEE J. Sel. Topics Appl. Earth Observ. Remote Sens.*, vol. 8, no. 1, pp. 425-435, Jan. 2015.

[11] N. Rodriguez-Alvarez *et al.*, "Airborne GNSS-R wind retrievals using delay-Doppler maps," *IEEE Trans. Geosci. Remote Sens.* , vol. 51, no. 1, pp. 626-641, 2013.

[12] E. Valencia *et al.*, "Using DDM asymmetry metrics for wind Direction retrieval from GPS ocean-scattered signals in airborne experiments," *IEEE Trans. Geosci. Remote Sens.*, vol. 52, no. 7, pp. 3924-3936, 2014.

[13] D. A Walker, "Observations of tsunami "shadows": A new technique for assessing tsunami wave heights?," *Sci. of Tsunami Hazards.*, 14, pp. 3-11, 1996.

[14] O. A. Godin, "Air-sea interaction and feasibility of tsunami detection in the open ocean," *J. Geophys. Res.*, vol. 109, no. C05002, pp. 1-20, May, 2004.

[15] A. Awada, A. Khenchaf, and A. Coatanhay, "Frequency impact on the bistatic radar scattering from an ocean surface," in *Proc. IEEE Int. Geosci. Remote Sens. Symp. (IGARSS)*, pp. 4459-4462, 2007.